Journal of the mechanical behavior of biomedical materials 65 (2017) 824–830

Contents lists available at ScienceDirect

Journal of the Mechanical Behavior of Biomedical Materials

journal homepage: www.elsevier.com/locate/jmbbm

Material properties of bovine intervertebral discs across strain rates

Nicolas Newell*, Grigorios Grigoriadis, Alexandros Christou, Diagarajen Carpanen, Spyros D. Masouros

Department of Bioengineering, Imperial College London, UK

ARTICLE INFO

Keywords:
Intervertebral disc
spine
Finite element modelling
inverse methods
Collagen fibre
material properties

ABSTRACT

The intervertebral disc (IVD) is a complex structure responsible for distributing compressive loading to adjacent vertebrae and allowing the vertebral column to bend and twist. To study the mechanical behaviour of individual components of the IVD, it is common for specimens to be dissected away from their surrounding tissues for mechanical testing. However, disrupting the continuity of the IVD to obtain material properties of each component separately may result in erroneous values. In this study, an inverse finite element (FE) modelling optimisation algorithm has been used to obtain material properties of the IVD across strain rates, therefore bypassing the need to harvest individual samples of each component. Uniaxial compression was applied to ten fresh-frozen bovine intervertebral discs at strain rates of 10^{-3}–1/s. The experimental data were fed into the inverse FE optimisation algorithm and each experiment was simulated using the subject specific FE model of the respective specimen. A sensitivity analysis revealed that the IVD's response was most dependent upon the Young's modulus (YM) of the fibre bundles and therefore this was chosen to be the parameter to optimise. Based on the obtained YM values for each test corresponding to a different strain rate ($\dot{\varepsilon}$), the following relationship was derived: $YM = 35.5 \ln \dot{\varepsilon} + 527.5$. These properties can be used in finite element models of the IVD that aim to simulate spinal biomechanics across loading rates.

1. Introduction

The intervertebral disc (IVD) is located between adjacent vertebral bodies of the spine and consists of three components; the nucleus pulposus (NP), annulus fibrosus (AF), and cartilaginous endplates (CEP). These components interact with one another such that the disc is able to distribute compressive loading on adjacent vertebral bodies, while allowing the vertebral column to bend and twist (Bogduk, 2005; Humzah and Soames, 1988). The functional anatomy of the IVD is determined by its complex material behaviour. As a viscoelastic structure, the IVD has material properties that are sensitive to strain rate (Virgin 1951). Capturing the behaviour of each of its components is important to understand better processes such as ageing, degeneration, and traumatic injury. It is also of importance for finite element (FE) simulations of the IVD or indeed the spine where accurate material models are essential to ensure valid predictions in mechanical response under loading.

Disrupting the continuity of the disc to test each component separately may have an effect on the obtained response and so result in erroneous material properties (Adams and Green, 1993). In particular, this is an issue for the most complex structure of the IVD, the AF, which incorporates concentric layers, known as lamella, with embedded fibres at alternating orientations. Inverse FE modelling provides the opportunity to obtain material properties of the individual components without disrupting the continuity of the IVD. The method involves developing an FE model with an accurate geometry, simulating a controlled experiment and then altering material properties until experimental and numerical responses of the IVD are in good agreement. This method has been used previously for other tissues that have complex interactions with surrounding components, for example the heel fat pad (Erdemir and Viveiros, 2006; Grigoriadis et al., 2017), the lung (Sadeghi Naini et al., 2011), and the cornea (Nguyen and Boyce, 2011), but, to the authors' knowledge, not the IVD.

Therefore, the aim of this study was to obtain material properties of components of the IVD at a range of loading rates without having to disrupt its structural integrity. We hypothesised that some components will have a greater influence on the IVD's mechanical response than others, and therefore, a specific objective was to perform a sensitivity study to identify these.

* Correspondence to: Dr Nicolas Newell, Department of Bioengineering, Imperial College London, South Kensington Campus, London SW7 2AZ, UK.
E-mail address: n.newell09@imperial.ac.uk (N. Newell).

http://dx.doi.org/10.1016/j.jmbbm.2016.10.012
Received 29 June 2016; Received in revised form 17 October 2016; Accepted 19 October 2016
Available online 19 October 2016

2. Methods

2.1. Specimen preparation

Ten vertebral body-disc-vertebral body (VB-disc-VB) specimens were harvested from six bovine tails that had been obtained from a local abattoir. Each specimen was Computed Tomography (CT) scanned (IVIS SpectrumCT Imaging System, Caliper Life Sciences, Hopkinton, MA, USA – voxel size 0.15×0.15×0.15 mm) to check for vertebral fractures or any other signs of pathology that may affect the properties of the IVD, and to allow accurate measurements of the geometry of the disc. Specimens were stored frozen at −20°C and each tail was thawed overnight at room temperature before dissection and testing. Two separate motion segments were obtained from each tail by cutting transversely through the first, second and third caudal VBs at mid-height. Surrounding soft tissues were carefully removed leaving VB-disc-VB specimens. Throughout the preparation process specimens were regularly sprayed with phosphate buffered saline (PBS, 0.15 mol/l) to keep them hydrated.

Using a custom built alignment jig the superior VB of the specimen was positioned such that the mid-plane of the disc was parallel to the ends of, and centred within, a 90 mm diameter pot. The superior VB was then fixed in position using polymethyl-methacrylate (PMMA) bone cement before being turned upside down allowing the inferior VB to be lowered into a second pot and again secured into position using PMMA.

2.2. Experimental procedure

Experiments were carried out using a servo-hydraulic materials testing machine (8872; Instron, Canton, MA, USA). The potted specimens were placed into the testing machine with a custom designed hood that allowed the compressive load to be spread across the whole pot (Fig. 1). The cross-head was lowered until a small compressive load (~5N) was recorded by the testing machine indicating that the compression tup was in contact with the top pot. The specimen was subjected to three preconditioning cycles of compression from 10 to 50 N at 1 Hz. A similar preconditioning sequence has been used previously (Adam et al., 2015), and preliminary tests suggested that this range was sufficient to ensure a repeatable response. Following the preconditioning cycles, the specimen was subjected to a main cycle to 15% strain. This strain was determined for each individual specimen based upon central disc height measurements taken from the CT scans and was chosen to ensure that the disc was not damaged, thus enabling multiple tests on a single specimen. Each disc was compressed at four strain rates (0.001, 0.01, 0.1, and 1/s), again calculated from central disc height measurements taken from the CT scans. Preliminary investigations showed that a 5 min relaxation period between tests was sufficient to obtain a repeatable force-displacement response.

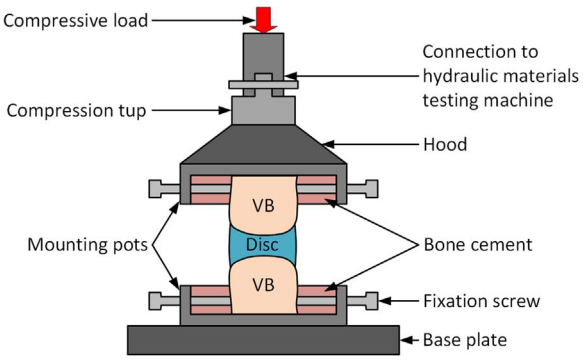

Fig. 1. Diagram of the experimental setup allowing compression of the VB-disc-VB specimen.

2.3. FE model development

Ten subject-specific, non-linear, implicit, axisymmetric FE models (MSC.Marc, v2015, MSC.Software, Santa Ana, CA, USA) were developed based on the CT scans of each specimen. The average of three measurements of the central disc height, peripheral disc height, and disc radius obtained from the CT scans were used to modify a generic geometry and ensure that the developed models were subject specific (Fig. 2). Internal geometry (NP:AF width ratio=3.72:1) and the number of lamellae (16) included in the model was based upon previous imaging studies of bovine IVDs (Adam et al., 2015). Fibre bundles in the AF were modelled using rebar elements while the AF matrix and NP were represented by quadrilateral 4-node axisymmetric elements. The fibre bundles were only present in the AF region of the disc and were assigned a constant Young's modulus in tension, but were not allowed to resist compression. The AF matrix and the NP were assigned non-linear hyperelastic material properties (Mooney-Rivlin). The strain energy function for this material model is shown in Eq. (1), where W is the strain-energy density function, I_1 and I_2 are strain invariants, and C_{10} and C_{01} are material constants (Mooney, 1940):

$$W = C_{10}(I_1\text{-}3) + C_{01}(I_2\text{-}3) \quad (1)$$

The fibre bundles were aligned at ± 30° to the transverse plane. The cross-sectional area of each bundle was assigned to be 3.212×10^{-2} mm, and spacing of the bundles was set to 0.23 mm or 4.35 bundles/mm (Adam et al., 2015; Marchand and Ahmed, 1990). Average element edge length ranged between 1.0 and 1.2 mm for the ten models and the results from a mesh convergence study ensured that this mesh density was sufficient. The discs were assumed to have vertical sides prior to loading although were allowed to bulge during the simulation, this assumption has previously been proven to be reasonable for bovine IVDs through assessment of polarised light micrographs (Adam et al., 2015). A preliminary numerical investigation demonstrated that modelling the endplates and vertebral bodies as deformable bodies with material properties from the literature (*YM* of cortical bone=11300 MPa, ν =0.2 (Little et al., 2007; Lu et al., 1996), *YM* of trabecular bone=140 MPa, ν=0.2 (Little et al., 2007; Lu et al., 1996), *YM* of endplate=23.8 MPa, ν=0.4 (Belytschko et al., 1974; Ueno and Liu, 1987; Yamada, 1970)), or rigid structures made little difference to the peak force (< 2.5%) or the final central disc height (< 0.9%) when a displacement that caused the disc to strain approximately 15% was applied at a range of strain rates. Therefore, to reduce computational cost, VBs and endplates were not modelled separately and were represented by rigid curves (Fig. 2).

The input to the model was the displacement-time history profile of the superior VB that was calculated from the displacement data recorded by the testing machine and was applied via a 'control node' to the upper rigid boundary. Apart from the VBs and the endplates, bone cement and pots were also assumed to be rigid since their stiffness is much greater than the components of the disc; therefore, the inferior boundary of the IVD was fixed while the superior boundary was assumed to have the same kinetic response as the compression tup in the experimental setup. Since the model was axisymmetric, nodes along the axis of symmetry (shown by the dotted lines in Fig. 2) were fixed in the radial direction.

2.4. Sensitivity study

A sensitivity study, to assess the contribution of the material properties of the various components of the IVD to its behaviour was conducted by adjusting the initial material properties, taken from literature (Table 1), by ± 20% on one of the subject-specific models that was selected due to its typical geometry (Specimen 1). Each property was adjusted one-at-a-time such that its effect on the force-time response could be determined. For the sensitivity study an intermediate strain rate was used (0.1/s).

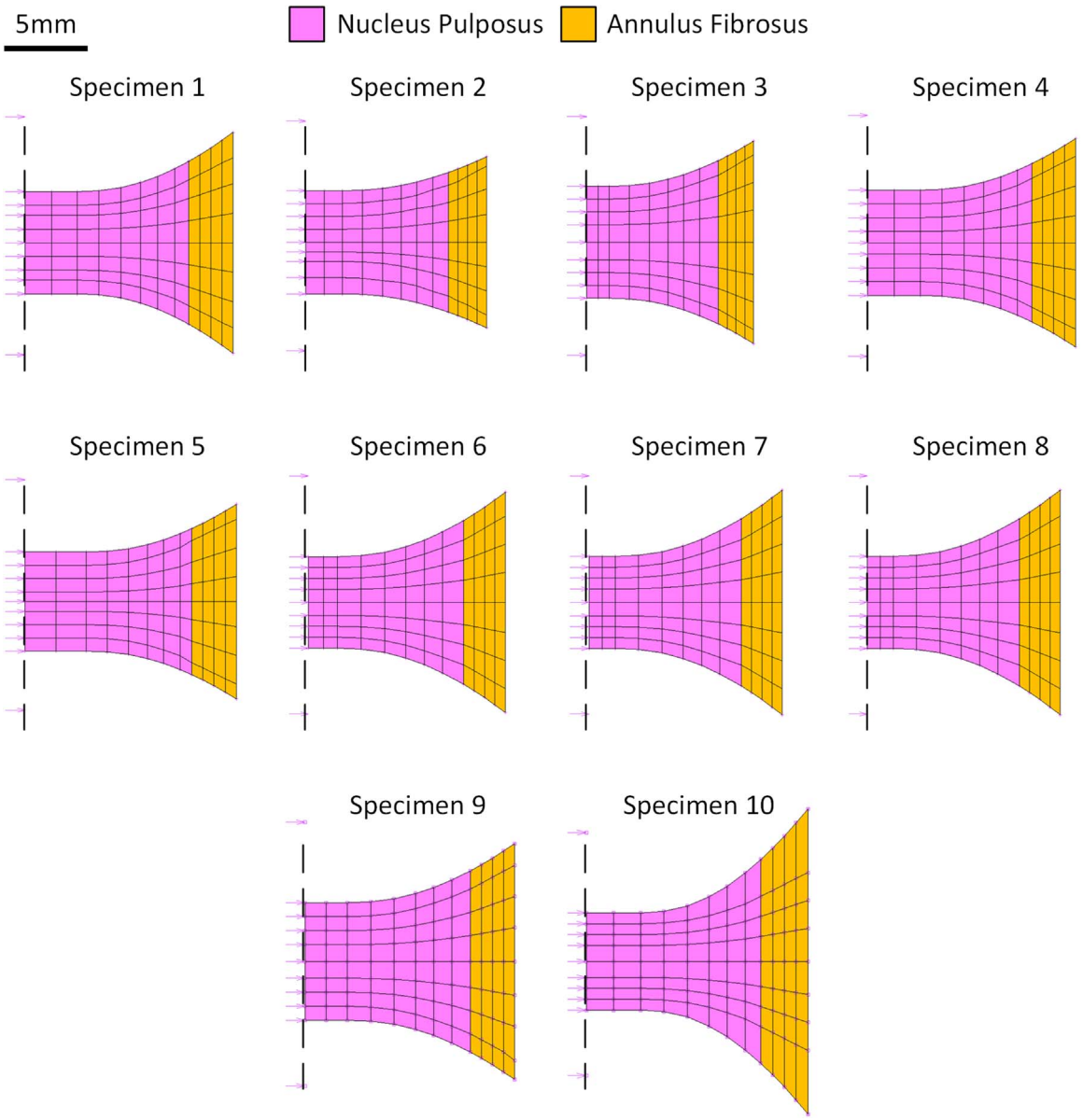

Fig. 2. Subject-specific, axisymmetric FE models of the ten bovine disc specimens. The dashed lines represent the axis of symmetry for each model. The upper rigid boundary of the disc was assigned a displacement to simulate each experiment and the lower rigid boundary was fixed. Rebar elements are not visualised in these figures but are within the AF matrix elements that are visible.

Table 1
Material properties used for the sensitivity study and as initial values for the optimisation study.

Component	Material model	Material parameters	Ref.
Collagen fibre bundles	Linearly elastic	500 MPa	Ueno and Liu (1987)
AF ground substance	Hyperelastic	C_{10}=0.7, C_{01}=0.2	Natali and Meroi (1990)
Nucleus pulposus	Hyperelastic	C_{10}=0.07, C_{01}=0.02	Adam et al. (2015)

2.5. Optimisation of the material properties

Following the sensitivity study it was found that the collagen fibre bundle material properties dominated the behaviour of the IVD and therefore only the Young's modulus of the AF fibre bundles were optimised. Their initial values were based on previous experimental studies (Table 1), before being optimised using a non-linear inverse FE optimization algorithm. The algorithm is based on the derivative-free Nelder-Mead or downhill-simplex method for function minimisation (Nelder and Mead, 1965). Experimental and numerical results were compared using the force measured above the specimen over time. Each test was simulated numerically while the Young's modulus value of the AF fibres was altered until a match between the numerical and experimental force-time data was achieved. An objective function was used to calculate the difference between numerical and experimental data and was minimised through the optimisation procedure. The optimisation was terminated when a) alterations of the fibre *YM* value had an effect smaller than 10^{-5} on the objective function; b) the difference between fibre *YM* values suggested through consecutive optimisation iterations was less than 10^{-5}; or c) the number of optimisation iterations reached 5000. The permissible range of values for the *YM* of the AF fibres during optimisation was restricted to 0.001–5000 MPa, thus ensuring that the resulting value would be physiologically acceptable. This optimisation process resulted in a fibre *YM* for each specimen, at each strain rate. The values were averaged at

Table 2
Dimensions for each of the ten subject-specific models. Central disc height, peripheral disc height and disc width values were taken from CT scans of the specimens while the AF width was calculated as a ratio of the total disc width (NP:AF ratio, 3.72:1 – Adam et al. (2015)). The numbers in brackets represent one standard deviation.

Specimen number	Central disc height (mm)	Peripheral disc height (mm)	Disc width (mm)	AF width (mm)
1	7.0	15.1	28.4	3.0
2	7.6	12.6	26.6	2.8
3	8.2	14.9	24.5	2.6
4	7.2	14.3	28.4	3.0
5	7.0	13.8	29.9	3.2
6	5.8	14.0	24.9	2.6
7	5.9	14.3	24.6	2.6
8	5.6	12.6	24.6	2.6
9	7.5	15.0	26.6	2.8
10	6.2	19.4	28.2	3.0
Average	6.8 (0.9)	14.6 (1.9)	26.7 (2.0)	2.8 (0.2)

each strain rate and differences between the means at each strain rate were determined using ANOVA, analysed post hoc using a Games-Howell test with the significance level set at p=0.05 (SPSS Statistics, Version 22.0, IBM Corp., Armonk, NY).

3. Results

3.1. FE model geometry

Dimensions of each specimen measured from the CT scans are shown in Table 2. These values were used to develop the subject-specific models shown in Fig. 2.

3.2. Experimental results

Force-displacement graphs for each of the specimens at each strain rate are shown in Fig. 3.

In order to analyse the strain-rate dependence of the IVDs the stiffness was calculated at three points along the curve (5, 10 and 15% strain). The averaged stiffness at each of these strains, at each strain rate is shown in Fig. 4.

3.3. Sensitivity study

The change in peak force seen when each of the material parameters was changed by ± 20% is shown in Fig. 5. The Young's modulus of the AF fibre bundles had the greatest influence on the behaviour of the disc (Fig. 5(i)). By comparison, the model was relatively insensitive to any of the NP material properties, any of the AF matrix properties, or the shear modulus, G of the AF fibres.

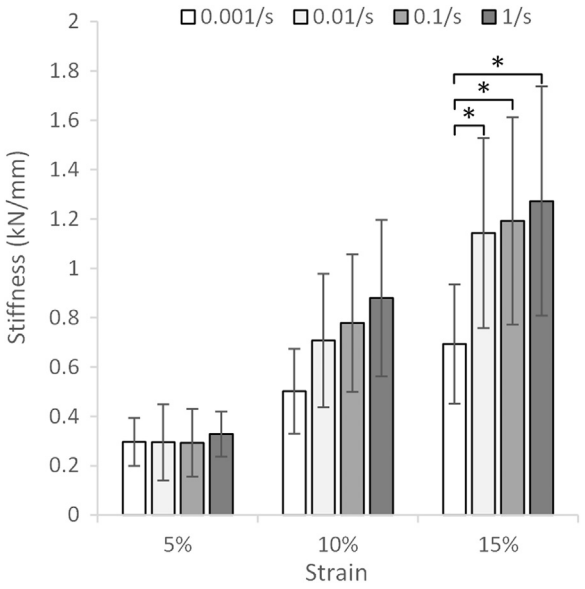

Fig. 4. Average stiffness at 5, 10 and 15% strain for each strain rate. *represents a statistical difference using ANOVA, analysed post hoc using a Games-Howell test with the significance level set at $p < 0.05$.

3.4. Optimisation

The optimised Young's modulus of the AF fibres ranged from 125 to 799 MPa and averaged 277 ± 95 MPa, 388 ± 185 MPa, 415 ± 149 MPa, and 540 ± 164 MPa, for strain rates of 0.001, 0.01, 0.1 and 1/s, respectively (Fig. 6). A significant difference was seen between the Young's moduli obtained at 0.001 and 1/s (p=0.038) but not between the Young's moduli obtained at any other strain rates ($p > 0.05$). A logarithmic curve was fit to the data in order to obtain a relationship between strain rate ($\dot{\varepsilon}$–s^{-1}) and the Young's modulus (YM - MPa) (Eq. 2). The R^2 value for this fit was 0.9515.

$$YM = 35.5 \ln \dot{\varepsilon} + 527.5 \quad (2)$$

4. Discussion

The motivation of this work was to obtain material properties of the individual components of the IVD without separating them from their surrounding tissues and therefore risking disrupting material continuity. This was achieved by using an inverse FE approach; this, to our knowledge, has been attempted for the first time on the IVD.

Bovine IVDs were chosen in this study as they offer two distinct

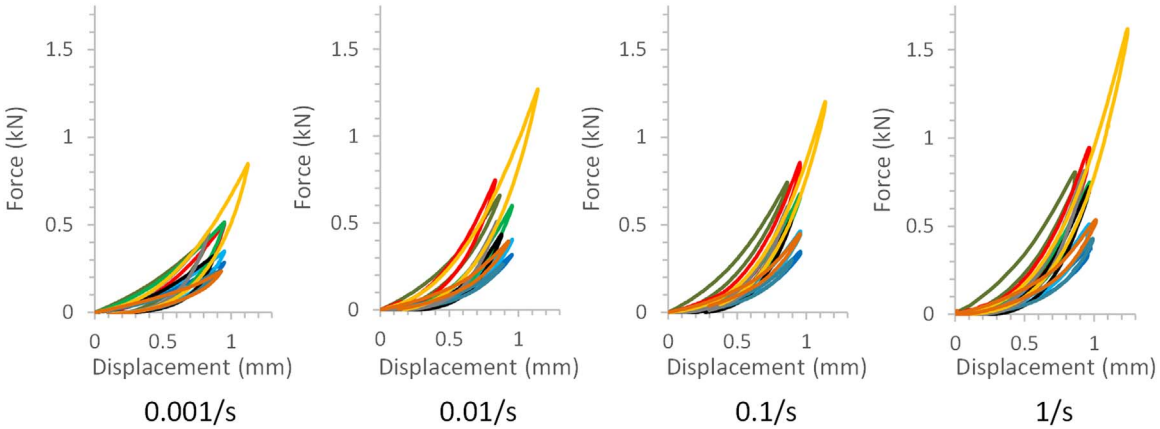

Fig. 3. Force-displacement graphs for each of the ten specimens at (a) 0.001/s, (b) 0.01/s, (c) 0.1/s and (d) 1/s. Each sample is represented by the same colour across strain rates.

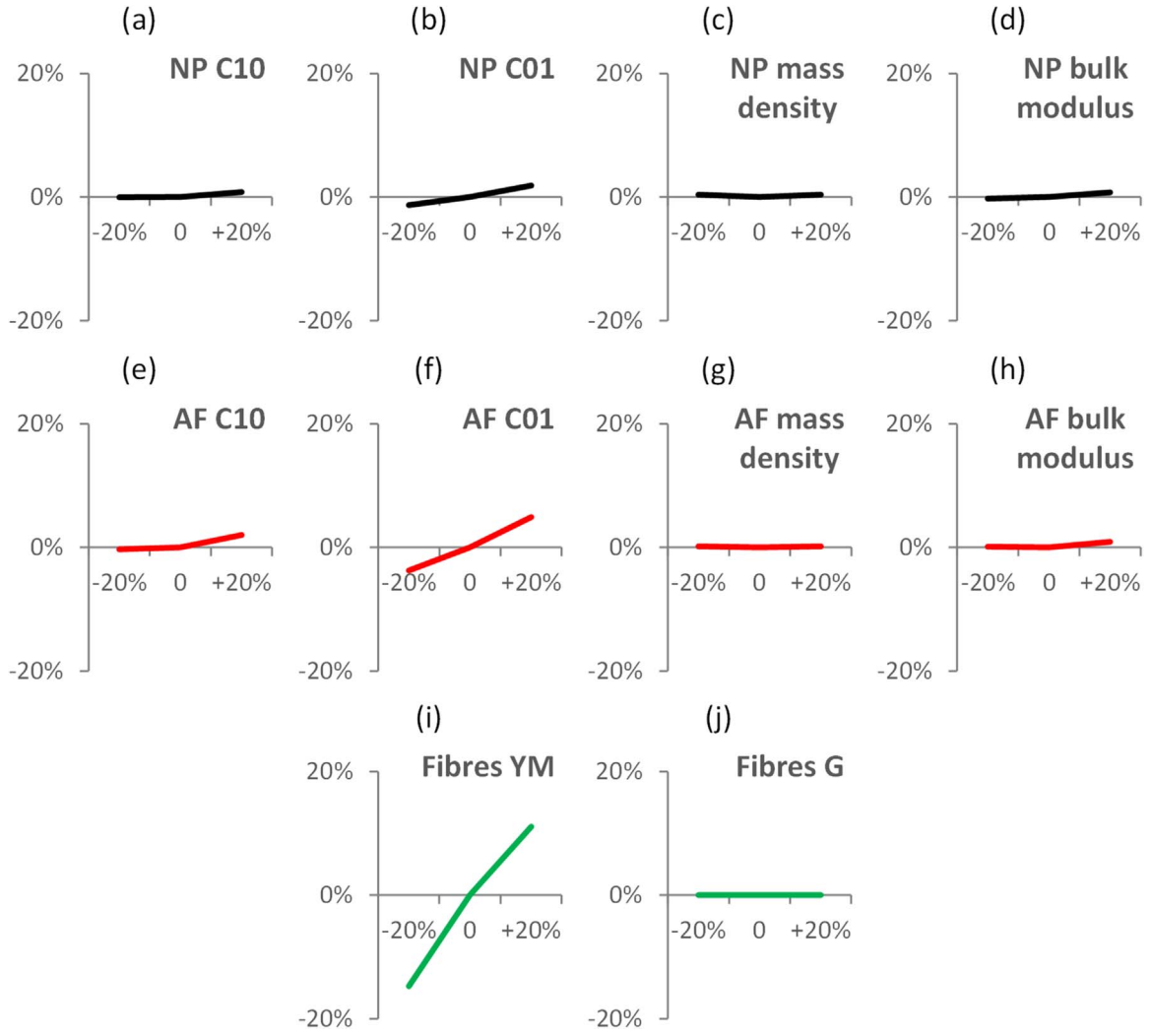

Fig. 5. Sensitivity study overview. The y–axis represents a percentage change in peak axial force from that obtained from the initial baseline run of the model when a parameter was changed by ± 20%. (a–d) are NP properties, (e–h) are AF matrix properties and (i–j) are AF fibre material properties.

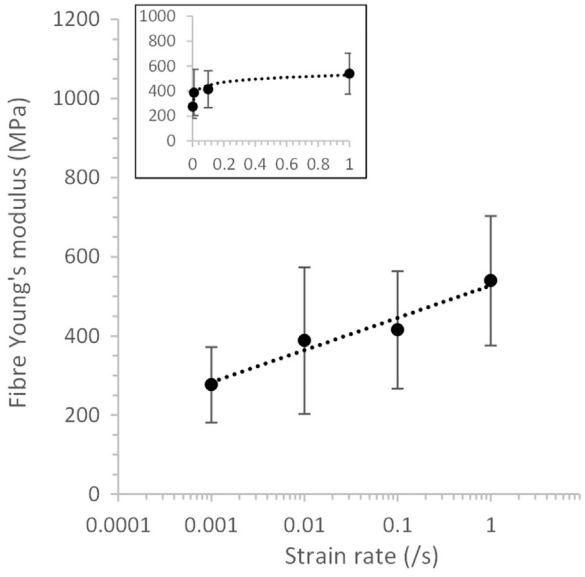

Fig. 6. Averaged optimised AF fibre Young's modulus for each of the ten subject-specific models at each strain rate. Note the logarithmic scale on the x–axis of the larger graph. The same data are presented with an x–axis that has a linear scale in the small, insert graph. The fit, described by Eq. (2) is represented by the dotted line. Error bars represent ± one standard deviation.

advantages over human specimens. Firstly, young, healthy bovine specimens are readily available, negating the complicating factor of IVD degeneration which is common in older human specimens (Race et al., 2000), and secondly, the transverse cross-section of the bovine IVDs is almost perfectly round (Adam et al., 2015; O'Connell et al., 2007), and therefore can be represented by a simple axisymmetric geometry. The mechanical response of bovine specimens has been found to be similar to that of human specimens, suggesting that disc tissue material properties are similar across species (Beckstein et al., 2008). Although the material properties of the bovine college fibre bundles derived in this study are likely to be appropriate for implement in FE models of the human spine, further tests on human IVDs are required to ascertain this hypothesis.

In agreement with the experimental results of Race et al. (2000) and Kemper et al. (2007), this study has shown that loading rates influence the mechanical response of the IVD (Fig. 4). No differences were seen in disc stiffness at each strain rate at 5 or 10% strain, however, at 15% strain differences in stiffness were significant between results from the lowest rate (0.001/s) and all other rates (0.01, 0.1, and 1/s), but no significant differences were seen between any of the higher loading rates (0.01, 0.1, and 1/s). Therefore, this study supports the findings of Race et al. (2000) who found a rate above which the strain-rate sensitivity was negligible. In this study, this rate was found to be at 0.01/s which corresponded to a loading rate of 75 N/s which is similar to the loading rate of 90 N/s found by Race et al. (2000).

The Young's modulus for the fibre bundles found here (277–540 MPa) is similar to values of 357-550 MPa that have been used in finite element models (Kiapour et al., 2012; Little et al., 2008; Ueno and Liu, 1987), and values of 100-470 MPa that have been measured in experiments of single collagen type I fibres isolated from rat tendons (Dutov et al., 2016), the dermis of sea cucumber (Shen et al., 2011, 2010), and bovine Achilles tendons (van der Rijt et al., 2006). Experiments that have involved tensioning AF specimens harvested from single lamellae along the axis of the fibres have been attempted previously (Holzapfel et al., 2005; Pezowicz et al., 2005; Skaggs et al., 1994). The samples tested in these experiments were a combination of AF matrix and fibre bundles; the modulus of those samples was found to be in the range of 28–136 MPa. In order to compare our results with these experiments we calculated an equivalent modulus of an AF specimen consisting of matrix and fibre bundles as follows: assuming 1) linear AF matrix properties of 0.814 MPa (Little et al., 2010), 2) fibre bundle cross-sectional area and spacing calculated from the measurements taken by Marchand and Ahmed (1990), and 3) samples with the geometry in Holzapfel et al. (2005) (average width=3.90 mm and thickness=0.56 mm), and using the fibre modulus of 277-540 MPa found in this study, the equivalent modulus of an AF sample consisting of matrix and fibre bundles is in the region of 49-95 MPa; this is comparable to the experimental results mentioned above (28–136 MPa). For the purposes of modelling the IVD accurately insofar as ensuring that the load being transferred through it is correct, the values presented here are more useful than those of AF specimens since it is common for fibre bundles and AF matrix to be separate materials in finite element models.

There were some simplifications with the geometry of the models of the discs used in this study; we assumed an NP:AF ratio based on imaging of other bovine discs (Adam et al., 2015), the fibre orientation was based upon previous studies (Marchand and Ahmed, 1990), and there was no initial disc bulge (at the outer AF or at the AF-NP boundary). Furthermore, all FE models that the authors are aware of define a clear boundary between the AF and the NP when in reality this boundary is not so distinct. In addition, in the majority of FE models, the lamellae are represented by concentric rings when in reality some are circumferentially discontinuous (Adam et al., 2015; Marchand and Ahmed, 1990). Similarly, there were some simplifications in the material models assigned; the AF fibres had no initial stress, and there was no initial pressure modelled in the NP. The sensitivity analysis performed in this study also suggests that only the AF fibre properties would need to be adjusted since their contribution to disc behaviour is far greater than any other material entity in the disc. Therefore, the potential geometrical and material inaccuracies mean that one must be cautious when using the material properties obtained here for other modelling configurations.

Experiments were conducted and modelled in pure axial compression in this study. The fibre bundles in the AF have been suggested to be under large strains in bending and twisting (Jensen, 1980), and therefore optimising the material properties for these modes of loading is an obvious direction for future studies. Furthermore, the methodology that was used successfully to characterise the behaviour of bovine IVDs in this study could be also applied for obtaining material properties of human IVDs by developing and using subject-specific 3D FE models.

5. Conclusions

The properties of the angled fibre bundles in the annulus fibrosus were found to dominate the behaviour of the IVD under axial compression. An optimisation algorithm utilising an inverse-FE technique performed on subject-specific models estimated the mean (± SD) Young's modulus of the fibre bundles to be 277 ± 95 MPa, 388 ± 185 MPa, 415 ± 149 MPa, and 540 ± 164 MPa, for strain rates of 0.001, 0.01, 0.1 and 1/s, respectively. The following relationship can be used for the Young's modulus (YM - MPa) of type I fibre bundles as a function of strain rate ($\dot{\varepsilon}$–s^{-1}): $YM = 35.5 \ln \dot{\varepsilon} + 527.5$. These values compare well with previous studies that have performed tensile tests on collagen type I fibre bundles, and, as expected are greater than the values obtained from tensile tests on single lamella anulus specimens which represent the combined response of fibre bundles and matrix.

Acknowledgements

This work was supported by the EPSRC, First Grant Scheme, EP/M022242/1. Contributions to this work were made under the auspices of The Royal British Legion Centre for Blast Injury Studies at Imperial College London; therefore the financial support of the Royal British Legion for GG, AC, DC, and SM is gratefully acknowledged. The financial support of the Medical Research Council (MR/K500793/1) for GG is also kindly acknowledged. Supporting data is available via Zenodo at http://dx.doi.org/10.5281/zenodo.163391. This data is available under a Creative Commons CC-BY license.

References

Adam, C., Rouch, P., Skalli, W., 2015. Inter-lamellar shear resistance confers compressive stiffness in the intervertebral disc: an image-based modelling study on the bovine caudal disc. J. Biomech. 48, 4303–4308. http://dx.doi.org/10.1016/j.jbiomech.2015.10.041.

Adams, M.A., Green, T.P., 1993. Tensile properties of the annulus fibrosus. I. The contribution of fibre-matrix interactions to tensile stiffness and strength. Eur. Spine J. 2, 203–208. http://dx.doi.org/10.1007/BF00299447.

Beckstein, J.C., Sen, S., Schaer, T.P., Vresilovic, E.J., Elliott, D.M., 2008. Comparison of animal discs used in disc research to human lumbar disc: axial compression mechanics and glycosaminoglycan content. Spine 33, E166–E173. http://dx.doi.org/10.1097/BRS.0b013e31824d911c, (Phila. Pa. 1976).

Belytschko, T., Kulak, R.F., Schultz, a B., Galante, J.O., 1974. Finite element stress analysis of an intervertebral disc. J. Biomech. 7, 277–285. http://dx.doi.org/10.1016/0021-9290(74)90019-0.

Bogduk, N., 2005. Clinical Anatomy of the Lumbar Spine and Sacrum Fourth ed.. Elsevier Health Sciences.

Dutov, P., Antipova, O., Varma, S., Orgel, J.P.R.O., Schieber, J.D., 2016. Measurement of elastic modulus of collagen type I single fiber. PLoS One 11, e0145711. http://dx.doi.org/10.1371/journal.pone.0145711.

Erdemir, A., Viveiros, M., 2006. An inverse finite-element model of heel-pad indentation. J. Biomech. 39, 1279–1289.

Grigoriadis, G., Newell, N., Carpanen, D., Christou, A., Bull, A., Masouros, S., 2017. Material properties of the heel fat pad across strain rates. J. Mech. Behav. Biomed. Mater. 65, 398–407.

Holzapfel, G.A., Schulze-Bauer, C.A.J., Feigl, G., Regitnig, P., 2005. Single lamellar mechanics of the human lumbar anulus fibrosus. Biomech. Model. Mechanobiol. (3), 125–140. http://dx.doi.org/10.1007/s10237-004-0053-8.

Humzah, M.D., Soames, R.W., 1988. Human intervertebral disc: structure and function. Anat. Rec. 220, 337–356. http://dx.doi.org/10.1002/ar.1092200402.

Jensen, G.M., 1980. Biomechanics of the lumbar intervertebral disk: a review. Phys. Ther. 60, 765–773.

Kemper, A.R., McNally, C., Duma, S.M., 2007. The influence of strain rate on the compressive stiffness properties of human lumbar intervertebral discs. Biomed. Sci. Instrum. 43, 176–181.

Kiapour, A., Ambati, D., Hoy, R.W., Goel, V.K., 2012. Effect of graded facetectomy on biomechanics of dynesys dynamic stabilization system. Spine 37, E581–E589. http://dx.doi.org/10.1097/BRS.0b013e3182463775, (Phila. Pa. 1976).

Little, J.P., Adam, C.J., Evans, J.H., Pettet, G.J., Pearcy, M.J., 2007. Nonlinear finite element analysis of anular lesions in the L4/5 intervertebral disc. J. Biomech. 40, 2744–2751. http://dx.doi.org/10.1016/j.jbiomech.2007.01.007.

Little, J.P., De Visser, H., Pearcy, M.J., Adam, C.J., 2008. Are coupled rotations in the lumbar spine largely due to the osseo-ligamentous anatomy?—A modeling study. Comput. Methods Biomech. Biomed. Eng. 11, 95–103. http://dx.doi.org/10.1080/10255840701552143.

Little, J.P., Pearcy, M.J., Tevelen, G., Evans, J.H., Pettet, G., Adam, C.J., 2010. The mechanical response of the ovine lumbar anulus fibrosus to uniaxial, biaxial and shear loads. J. Mech. Behav. Biomed. Mater. 3, 146–157. http://dx.doi.org/10.1016/j.jmbbm.2009.09.002.

Lu, Y., Hutton, W., Gharpuray, V., 1996. Do bending, twisting, and diurnal fluid changes in the disc affect the propensity to prolapse? A viscoelastic finite element model. Spine 21, 2570–2579, (Phila. Pa. 1976).

Marchand, F., Ahmed, A.M., 1990. Investigation of the laminate structure of lumbar disc anulus fibrosus. Spine 15, 402–410. http://dx.doi.org/10.1097/00007632-199005000-00011, (Phila. Pa. 1976).

Mooney, M., 1940. A theory of large elastic deformation. J. Appl. Phys. 11, 582–592.

Natali, A., Meroi, E., 1990. Nonlinear analysis of intervertebral disk under dynamic load. J. Biomech. Eng. 112, 358–363. http://dx.doi.org/10.1115/1.2891196.

Nelder, J., Mead, R., 1965. A simplex method for function minimization. Comput. J. 7,

308–313.
Nguyen, T.D., Boyce, B.L., 2011. An inverse finite element method for determining the anisotropic properties of the cornea. Biomech. Model. Mechanobiol. 10, 323–337. http://dx.doi.org/10.1007/s10237-010-0237-3.
O'Connell, G.D., Vresilovic, E.J., Elliott, D.M., 2007. Comparison of animals used in disc research to human lumbar disc geometry. Spine 32, 328–333. http://dx.doi.org/10.1097/01.brs.0000253961.40910.c1, (Phila. Pa. 1976).
Pezowicz, C.A., Robertson, P.A., Broom, N.D., 2005. Intralamellar relationships within the collagenous architecture of the annulus fibrosus imaged in its fully hydrated state. J. Anat. 207, 299–312. http://dx.doi.org/10.1111/j.1469-7580.2005.00467.x.
Race, A., Broom, N.D., Robertson, P., 2000. Effect of loading rate and hydration on the mechanical properties of the disc. Spine 25, 662–669. http://dx.doi.org/10.1097/00007632-200003150-00003, (Phila. Pa. 1976).
Sadeghi Naini, A., Patel, R.V., Samani, A., 2011. Measurement of lung hyperelastic properties using inverse finite element approach. IEEE Trans. Biomed. Eng. 58, 2852–2859. http://dx.doi.org/10.1109/TBME.2011.2160637.
Shen, Z.L., Dodge, M.R., Kahn, H., Ballarini, R., Eppell, S.J., 2010. In vitro fracture testing of submicron diameter collagen fibril specimens. Biophys. J. 99, 1986–1995. http://dx.doi.org/10.1016/j.bpj.2010.07.021.
Shen, Z.L., Kahn, H., Ballarini, R., Eppell, S.J., 2011. Viscoelastic properties of isolated collagen fibrils. Biophys. J. 100, 3008–3015. http://dx.doi.org/10.1016/j.bpj.2011.04.052.
Skaggs, D.L., Weidenbaum, M., Iatridis, J.C., Ratcliffe, A., Mow, V.C., 1994. Regional variation in tensile properties and biochemical composition of the human lumbar anulus fibrosus. Spine 19, 1310–1319. http://dx.doi.org/10.1097/00007632-199406000-00002, (Phila. Pa. 1976).
Ueno, K., Liu, Y.K., 1987. A three-dimensional nonlinear finite element model of lumbar intervertebral joint in torsion. J. Biomech. Eng. 109, 200–209.
van der Rijt, J.A.J., van der Werf, K.O., Bennink, M.L., Dijkstra, P.J., Feijen, J., 2006. Micromechanical testing of individual collagen fibrils. Macromol. Biosci. 6, 697–702. http://dx.doi.org/10.1002/mabi.200600063.
Yamada, H., 1970. Strength of Biological Materials. Williams & Wilkins, Baltimore, MD, USA.